# Road to disorder in smectic elastomers

Evgeny P. Obraztsov,[1] Adrian S. Muresan,[1] Boris I. Ostrovskii,[1,2] and Wim H. de Jeu[1,*]
[1]*FOM Institute for Atomic and Molecular Physics, Kruislaan 407, 1098 SJ Amsterdam, Netherlands*
[2]*Institute of Crystallography, Academy of Sciences of Russia, Leninsky Prospect 59, 117333 Moscow, Russia*
(Received 27 August 2007; published 28 February 2008)

We present a high-resolution x-ray study of the effects of disorder induced by random cross-linking side-chain smectic elastomers. The influence of variation of the concentration and stiffness of the cross-link units on the disruption of the one-dimensional translational order is reported in detail. Precise analysis of the line shape of the quasi-Bragg peaks associated with the smectic layering indicates a transition from algebraic decaying ordering to disorder. The smectic line shapes can be described by the Caillé correlation function convoluted with a finite-size factor represented by a stretched Gaussian (compressed exponential). The transition to disorder is signaled by a change in the exponent of the stretched Gaussian from 1 (simple Gaussian describing finite-size domains) via 0.5 (Lorentzian describing exponentially decaying short-range correlations) to $<0.5$ (stretched exponential correlations). For a flexible cross linker the changeover occurs for concentration between 0.15 and 0.20, for a stiff cross linker below about 0.10. Broadening of the higher harmonics of the x-ray peak indicates strong nonuniform strain within finite-size domains and local deformations induced by randomly distributed dislocations.

DOI: 10.1103/PhysRevE.77.021706 PACS number(s): 61.30.Eb, 64.60.Cn, 61.05.cf, 61.41.+e

## I. INTRODUCTION

The effect of randomness and disorder in condensed matter remains an intriguing and challenging problem, relevant to physical systems containing either specific types of defect or placed in a random environment [1]. Examples are rather different and include the pinning of an Abrikosov flux vortex lattice by impurities in superconductors [2], disordered Ising magnets [3], superfluid transitions of $He^4$ in a porous medium [4], and phase transitions in smectic liquid crystals in a random confinement [5]. Regarding the first example Larkin [6,7] predicted that at large enough length scales even a weak random field should destroy translational order below four dimensions, resulting in exponentially decaying positional correlations. Later work [8] recognized that the effect of the disorder was overestimated and that quasi-long-range order can survive (positional correlations decaying algebraically at large distances). This latter property is similar to the behavior of solids in two dimensions as well as of the layer correlations in smectic liquid crystals (LC) [9]. Monomer and polymer smectic LC phases consist of stacks of liquid layers in which thermally excited fluctuations cause the mean-squared layer displacements to diverge logarithmically with the system size (Landau-Peierls instability) [10,11]. As a result the positional correlations decay algebraically as $r^{-\eta}$, $\eta$ being small and positive, and the discrete Bragg peaks change into singular diffuse scattering with an asymptotic power-law form [12]. This type of anisotropic line shape was first observed in low-molecular-mass thermotropic smectic phases by Als-Nielsen *et al.* [13] and then also for lyotropic lamellar phases [14–16], smectic polymers [17], and lamellar block copolymers [18]. Quenched disorder has been introduced in smectic monomer systems by confinement in the voids presented by the connected filaments of an aerogel or alternatively by dispersion of hydrophilic aerosil. Even at very low density of the aerogels or aerosils (about 1%–3%) the one-dimensional (1D) smectic order is destroyed and persists only locally on a length scale of the order of 100 nm [5,19–21]. This behavior is in agreement with general theoretical predictions that any quenched disorder should do so, no matter how weak [22,23].

In the present work we consider smectic elastomers in which disorder is introduced by the random network of cross links. Liquid crystalline order and polymer properties can be combined by attaching mesogenic molecules to a polymer backbone via flexible linkages (side-chain LC polymers). The backbone polymer—in turn—can be weakly cross linked to form an elastomer. The macroscopic rubber elasticity introduced via such a percolating network interacts with the LC ordering field [24]. In nematic elastomers orientational transitions driven by the soft rubber elasticity lead to forms of mechanical instabilities and orientational memory effects. Interestingly, their shape varies parallel to the changing levels of the nematic (orientational) order [25]. In smectic LC elastomers (see Fig. 1) the layers cannot move easily across the cross-linking points where the polymer backbone is attached. Consequently layer displacement fluctuations are suppressed, which effectively stabilizes the 1D periodic layer structure [26,27]. In agreement with these predictions reinstatement of true long-range order has been observed upon cross linking [28]. On the other hand, the cross links provide a random network of defects that could destroy the smectic order [29,30]. Thus, in smectic elastomers two opposing tendencies exist: the suppression of layer displacement fluctuations that enhances the translational order and the random quenched disorder that leads to a highly frustrated equilibrium state. In a preliminary report we demonstrated both tendencies [31]: Upon increasing the cross-link density, after an initial small decrease (ordering) the width of the quasi-Bragg peak corresponding to the layer structure strongly in-

*Present address: Polymer Science and Engineering, University of Massachusetts, 120 Governors Drive, Amherst, MA 01003, USA. E-mail: dejeu@mail.pse.umass.edu

 

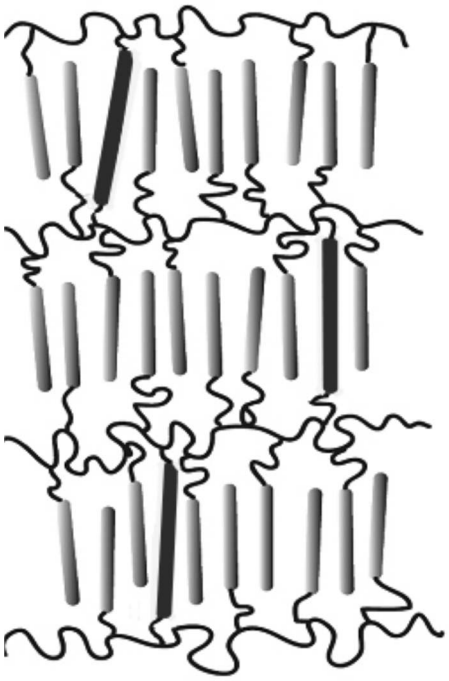

FIG. 1. Schematic picture of a smectic side-chain elastomer.

creases (disordering). Finally, at about 20% cross links, extended short-range order developed.

In this paper we report measurements that reveal in some detail the subtleties of the process of increasing disorder in smectic elastomers. The transition to disorder is reflected in the x-ray line shape by a change in the exponent of a stretched Gaussian from 1 (simple Gaussian describing finite-size domains) via 0.5 (exponentially decaying short-range correlations) to $<0.5$ (stretched exponential decay). In addition the width of the smectic quasi-Bragg peak increases with the harmonic number. This behavior does not follow the general line of theories of quenched random disorder (in contrast to confined smectic monomer systems), but rather points to considerable nonuniform internal strain within the smectic domains due to defects of the 1D lattice.

## II. EXPERIMENT

Smectic-*A* (Sm-*A*) polysiloxanes (Fig. 2) were synthesized as described elsewhere [32]. The average degree of polymerization was about 250 with a broad distribution typical of a polycondensation reaction. Both types of compounds (types I and II) contained as mesogenic groups benzoic acid phenylesters ($R_1$, $R_2$) and a cross-linking agent ($R_3$). Type II differed from type I by the presence of a second mesogenic group ($R_2$). In the following discussion we consider them as essentially one system. The standard cross link was a bifunctional nonmesogenic hydroquinone derivative ($V_1$); in addition a stiffer cross link $V_8$ was used. The elastomers and/or polymers were studied in the Sm-*A* phase at room temperature, well below their smectic-isotropic transition around 65 °C–75 °C (depending on cross-link density). The Sm-*A* phase was identified through a set of sharp (00*n*) quasi-

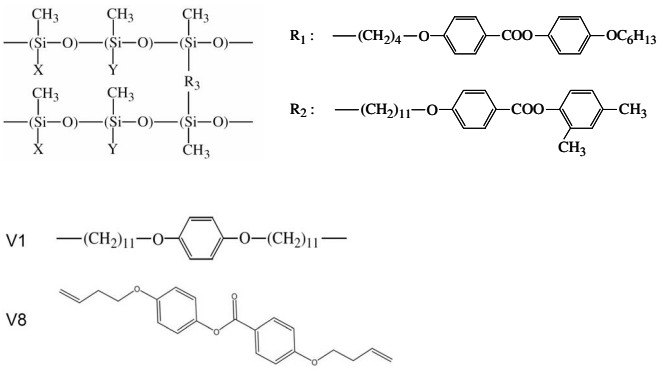


FIG. 2. Chemical structures. Elastomer type I has $X=Y=$R2; type II has $X=$R1 (45%) and $Y=$R2 (55%). The cross-link R3 is primarily given by V1; alternatively by the more rigid V8.

Bragg peaks along the layer normal at a wave vector $q_n$ and a broad liquidlike peak from the in-plane short-range order. Oriented elastomer samples (typically $40\times 10$ mm$^2$ and 0.5 mm thick) were obtained through uniaxial deformation during the cross-linking process. This determined the long direction of the sample (coinciding with the smectic layer normal) which was fixed during the completion of the network. Homopolymer films were prepared at temperatures close to the smectic-isotropic transition by moving a spreader over a glass substrate to give films a thickness of about 100 $\mu$m and a mosaic distribution of the layer normal $\lesssim 1.5°$.

The experiments were performed at the Exxon beamline X10A at the National Synchrotron Light Source, Brookhaven National Laboratory, using 8 keV radiation (wavelength $\lambda=0.155$ nm). To observe the power-law singularities of the smectic structure factor $S(q)\sim(q_z-q_n)^{-2+n^2\eta}$, the x-ray setup should be used at high resolution, capable of measuring length scales of the order of micrometers together with a steep fall-off of the tails of the resolution function [13]. These requirements were fulfilled by a diffractometer equipped with a double-bounce Ge(111) monochromator and a triple-pass channel-cut Ge(220) or Si(111) analyzer crystal. In practice the tails fall down according to $\sim(q_z-q_n)^{-4.5}$ at small deviations from the Bragg position and $\sim(q_z-q_n)^{-3}$ further away. The wave-vector transfer is given by $\mathbf{q}=\mathbf{k}_f-\mathbf{k}_i$, where $\mathbf{k}_f$ and $\mathbf{k}_i$ are the outgoing and incoming wave vector, respectively, with $q=|\mathbf{q}|=(4\pi/\lambda)\sin\theta$, $2\theta$ being the scattering angle. The scattering plane ($z,x$ plane) was vertical with the $q_z$ axis parallel to the smectic layer normal. Hence the quasi-Bragg peaks were measured in reciprocal space along $q_z$ while the mosaic distribution was determined by transverse (rocking) curves varying $q_x$ at different $q_z=q_n$. The resolution function in the scattering plane was close to a Gaussian with $\Delta q_z=0.003$ nm$^{-1}$ [full width at half-maximum (FWHM)]. The resolution function along the $q_x$ direction was an order of magnitude narrower and could be taken as a $\delta$ function. Hence the peak width in this direction was directly due to the mosaic distribution $\phi$ giving $\Delta q_x\cong q_n\phi$. Out of the scattering plane the resolution was set by slits to $\Delta q_y=0.02$ nm$^{-1}$. The incident intensity was about $5\times 10^9$ cts/s; the beam size was $0.5\times 1$ mm$^2$ ($V\times H$). All data were normalized, resolution corrected, and background

subtracted. The latter point is a crucial aspect for the present precise line-shape measurements including the tails of the peaks. In particular it requires separate consideration of the **q**-dependent spatial background in the hutch and the time-dependent dark current of the scintillation counter.

## III. MODELING

### A. Theoretical background

The elastic free energy of a smectic system is concerned with the layer displacement field $u(\mathbf{r})=u_z(\rho,z)$ along the layer normal $z$. A conventional smectic with liquid layers has no resistance to shear, and a term $[\nabla_\perp u(r)]^2$ is not allowed in the deformation energy. Only higher-order contributions $\sim[\Delta_\perp u(r)]^2$, corresponding to layer curvature, are energetically penalized. As a result in the long-wavelength limit $q\to 0$ fluctuation modes have a large amplitude. In the harmonic approximation the equipartition theorem gives for each mode of layer displacement $u(\mathbf{q})$ the mean-square value

$$\langle u^2(\mathbf{q})\rangle = \frac{k_BT}{Bq_z^2 + Kq_{xy}^4}. \tag{1}$$

Here $u(\mathbf{q})$ is the Fourier transform of the layer displacement field, the elastic moduli $K$ and $B$ describe bending and compression, respectively, of the smectic layers, $k_BT$ is the thermal energy while the subscript $xy$ refer to in-plane directions. As a result the mean-square fluctuations diverge logarithmically with the system size $L$ according to

$$\langle u^2(\mathbf{r})\rangle = \frac{k_BT}{8\pi\sqrt{KB}}\ln\left(\frac{L}{d}\right). \tag{2}$$

This expression can be contrasted with the finite amplitude of mean-squared fluctuations in a three-dimensional solid that take the form

$$\langle u^2(\mathbf{r})\rangle = \frac{k_BT}{\pi aC}, \tag{3}$$

in which $C$ is a typical elastic constant and $a$ is a lattice dimension.

For a smectic liquid crystal the structure factor $S(\mathbf{q})$ determining the scattering is related to the layer correlation function $G_n(\mathbf{r})$ by

$$S(\mathbf{q}) \propto \int d^3\mathbf{r} G_n(\mathbf{r})\exp[i(\mathbf{q}-\mathbf{q_n})\cdot\mathbf{r}], \tag{4}$$

in which

$$G_n(\mathbf{r}) = \langle\exp\{iq_z[u(\mathbf{r})-u(0)]\}\rangle. \tag{5}$$

In the harmonic approximation this can be written as

$$G_n(\mathbf{r}) = \exp\left(-\frac{1}{2}q_n^2\langle[u(\mathbf{r})-u(0)]^2\rangle\right). \tag{6}$$

The pair-correlation function describing the algebraic decay typical for the layer structure of a smectic liquid crystal has been given by Caillé [12] as

$$G_n(\mathbf{r}) = G_n(\rho,z) \propto \left(\frac{2d}{\rho}\right)^{2n^2\eta}\exp\left\{-n^2\eta\left[2\gamma_E + \mathrm{E}_1\left(\frac{\rho^2}{4\lambda z}\right)\right]\right\}. \tag{7}$$

In this expression $\gamma_E=0.5772\ldots$ is Euler's constant, $\mathrm{E_1}(x)$ is the exponential integral, and $r^2=z^2+\rho^2$ with $\rho^2=x^2+y^2$. The reciprocal lattice vectors are defined by $q_n=nq_0=2\pi n/d$ $(n=1,2,\ldots)$, and $\lambda=\sqrt{K/B}$ is the so-called penetration depth. The dimensionless index $\eta$ describing the algebraic decay $z^{-\eta}$ along the layer normal and $\rho^{-2\eta}$ inside the layers is given by

$$\eta = q_0^2\frac{k_BT}{8\pi\sqrt{BK}}. \tag{8}$$

It determines the well-known asymptotic power-law behavior along the layer normal,

$$(q_z) \propto (q_z - q_n)^{-(2-\eta_n)}, \quad \eta_n = n^2\eta. \tag{9}$$

There are a finite number of power-law singularities of the type of Eq. (9); when for large $q_n$ we arrive at $\eta_n>2$ they are replaced by cusplike peaks. The observed scaling behavior of $\eta_n$ on $n^2$ for the first- and higher-order harmonics is one of the strongest arguments in favor of Caillé's harmonic approach. The exponent in Eq. (8) is valid for a perfectly oriented sample. In the other limit of a powder distribution of orientations an exponent $1-\eta_n$ applies. In practical cases the transition between these two limits must be considered.

In a smectic elastomer the underlying elastic network couples to the layer displacements. Hence, the usual smectic degeneracy with respect to uniform layer rotations is lost, and a shear term occurs in the elastic energy. Though the resulting expression for the free energy as a function of layer displacements is rather complicated, the essential physics can be derived from the dispersion law for the elastomer phonon modes which now features a solidlike elastic energy proportional to an overall square power $\sim q^2$ [27]. As a result the fluctuation behavior can be described by

$$\langle u^2(\mathbf{r})\rangle = \frac{k_BT}{\pi d\sqrt{C_5^*B^*}}, \tag{10}$$

where $B^*$and $C_5^*$ are renormalized bulk compression and shear moduli, respectively. The expression is similar to Eq. (3), indicating suppression of the Landau-Peierls instability. This can lead to reestablishment of true long-range order, even though the translational order is still 1D, like in a non-cross-linked smectic polymer [26,27].

So far, the cross links—pinning the smectic layers in a number of points—were not supposed to alter the smectic density wave. However, the cross links are also expected to disturb the layer structure itself, which effect will become more important with increasing concentration. A preferential reduction of the smectic density around a cross link can be modeled by a local random field that adjusts the phase of the smectic density wave [29],

$$F_{\mathrm{RF}} = \sum_i \gamma |\psi(\mathbf{R}_i)| \cos[q_0(z_i) - u(\mathbf{R}_i)]. \tag{11}$$

Here $\psi(\mathbf{r})$ is the smectic order parameter and $\mathbf{R}_i$ the position of the $i$th cross link. This problem has been extensively investigated for quenched disorder (defects fixed in time and space) by group renormalization methods [22,23] as well as by replica symmetry breaking [8,29]. The results predict that even arbitrary weakly quenched disorder should destroy the 1D smectic order. The problem has been approached experimentally using highly porous silica aerogels or hydrophilic aerosils as a source of quenched disorder [5,19–21]. The experiments show that even a very low density of aerogels and/or aerosils destroys the 1D smectic order that persists only locally on a macroscopic length scale $\xi(T) \simeq 100$ nm, the x-ray correlation length. This length is not characteristic for the aerogel structure—as would be the case for a cutoff in standard porous materials—but results from the competition between the randomizing effect of the defect network and the smectic elastic field. Thus, there is no distinct Sm-$A$ phase and nematic–smectic-$A$ transition in such a system. In the smectic elastomers considered here the situation is rather different because the cross links are not rigidly frozen defects, but consist of flexible chains embedded in the slowly fluctuating elastomer gel.

### B. Semiphenomenological model

In a real nonideal smectic system in addition to the correlation function $G_n(\rho,z)$ various other effects contribute to the x-ray line shape. For a conventional smectic liquid crystal these are in principle well known and can be written in terms of the intensity $I(\mathbf{q})$ as

$$I(\mathbf{q}) \propto \int d^3\mathbf{r} G_n(\rho,z) H(\rho,z) F(\rho) R(x,y,z) \exp[i(\mathbf{q} - \mathbf{q_n}) \cdot \mathbf{r}]. \tag{12}$$

In this equation $H(\rho,z)$ describes finite-size effects, $F(\rho)$ represents the effect of the mosaic distribution of the sample, and finally $R(x,y,z)$ is the instrumental resolution function. We shall first summarize how these effects can be treated, following largely Ref. [33]. Then we discuss how harmonic-dependent strain—which in a phenomenological approach is the hallmark of cross linking—can be incorporated into $I(\mathbf{q})$.

In practice the stacking of smectic layers is limited: the maximal domain size layers is of the order of some tens of $\mu$m. This brings us to the second factor in Eq. (12), $H(\rho,z)$. Let us assume that the domain sizes along and perpendicular to the layer normal are independent. The finite size of each domain $m$ will affect the expression for the scattered intensity via an additional factor $H_m(\rho,z)$, which should be averaged over all domains to give the effective finite-size contribution $H(\rho,z)$. Let us assume that $H_m(\rho,z)$ corresponds to a domain with dimensions $L_x \times L_y \times L_z$ and sharp boundaries. Then its Fourier transform has the well-known form

$$H_m(\mathbf{q}' + \mathbf{q_n}) = \prod_{i=1}^{3} \frac{\sin^2(q_i' L_i/2)}{(q_i' L_i/2)^2}, \tag{13}$$

which corresponds in $\mathbf{r}$ space to a triangle $1 - |z|/L$ for each dimension. Hence, for this situation $H_m(\rho,z)$ can be used.

If the elastomer consists of domains of different size or the boundaries are not sharp, we can follow the Warren approximation [34] for finite lattice sums leading to Gaussian functions

$$H(\rho,z) \equiv H(\rho)H(z) = \exp[-\pi(\rho/L_\rho)^2 - \pi(z/L_z)^2]. \tag{14}$$

The distribution and magnitude of the domains along the layer normal as expressed in $H(z)$ are crucial for analysis of the line shape along the layer normal. The in-plane contribution depending on $L_\rho$ is less important. In fact it adds up with the contribution from the mosaic distribution and will be incorporated later. Depending on the specific situation, in particular the nature of the topology and the related defects, the domain-size distribution in $H(z)$ could become highly inhomogeneous with an associated probability function $P_H(L/L_0)$ with characteristic length $L_0$. Generally this means

$$H(z) = \int_0^\infty \frac{dL}{L_0} P_H(L/L_0) H_m(z) = \int_{|z|}^\infty \frac{dL}{L_0} P_H(L/L_0) \left(1 - \frac{|z|}{L}\right). \tag{15}$$

The following normalized probability function for the domain-size distribution has been chosen, which seemed plausible because of the stochastic nature of the domain formation,

$$P_H^\beta(L/L_0) = \frac{2\beta}{\Gamma[1 + 1/(2\beta)]} \left(\frac{L^2}{L_0^2}\right)^\beta \exp[-(L^2/L_0^2)^\beta]. \tag{16}$$

For this formula $L_0$ determines the most probable domain size (first derivative equals zero). For the specific cases $\beta = 0.5$ and $\beta = 1.0$, Eq. (16) reads as

$$P_H^{0.5}(L/L_0) = \frac{L}{L_0} \exp(-L/L_0), \tag{17}$$

$$P_H^{1.0}(L/L_0) = \frac{4}{\pi} \frac{L^2}{L_0^2} \exp(-L^2/L_0^2). \tag{18}$$

As we see $P_H^{0.5}(L/L_0)$ describes an exponential decay for domain sizes after averaging and a linear growth for small sizes. This distribution is very broad (solid line in Fig. 3); the same behavior has been obtained for a description of the distribution of end points of polymer brushes near an interface. $P_H^{1.0}(L/L_0)$ (dashed line in Fig. 3) does result in a somewhat complicated form with a Gaussian as leading term; hence it is relatively narrow. Finally for large $\beta$ values (strongly compressed Gaussian) Eq. (16) is close to a $\delta$ function (dotted line in Fig. 3). We note that similar approaches have been used in powder diffraction to describe the dispersion of grain sizes (see [35], and references therein).

When calculating the finite-size contribution, averaging of Eq. (15) gives after some algebraic operations

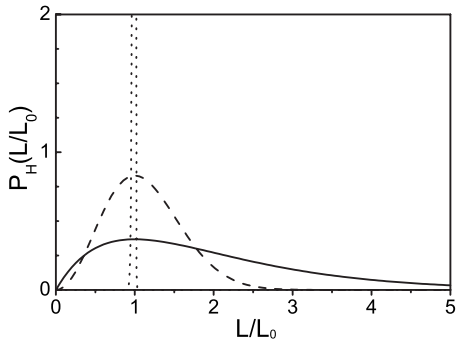


FIG. 3. Model domain size distributions. Full line corresponds to a distribution resulting in exponential decay ($\beta$=0.5), dashed line to a distribution resulting in a Gaussian ($\beta$=1.0), dotted line to a distribution close to a $\delta$ function ($\beta$=50).

$$H^{\beta}(z) = \exp\left[-\left(\frac{z^2}{L_0^2}\right)^{\beta}\right]\frac{1}{\Gamma\left(1+\frac{1}{2\beta}\right)} \times \int_1^{\infty} \exp\left[-\left(\frac{z^2}{L_0^2}\right)^{\beta}(\zeta^{2\beta}-1)\right]\frac{|z|}{L_0}d\zeta. \quad (19)$$

For $\beta$=0.5 this reduces to an exponential decay (see Fig. 4)

$$H(z) = \exp\left(-\frac{|z|}{L_0}\right).$$

For other $\beta$ values and $|z| > L_0$ the asymptotic behavior is as follows:

$$H^{\beta}(z) \sim \exp\left[-\left(\frac{z^2}{L_0^2}\right)^{\beta}\right]\left(\frac{|z|}{L_0}\right)^{1-2\beta}.$$

Restricting ourselves to the leading term we arrive at a stretched Gaussian function that can be written as

$$H(z) = \exp\left(-\frac{(\sigma_{\beta}z)^{2\beta}}{2\beta}\right). \quad (20)$$

As illustrated in Fig. 4, a Gaussian function (obtained for $\beta$=1) is closest to a distribution of triangular domains of well-defined size. The situation $0.5 < \beta < 1$ can be described as a stretched Gaussian or equivalently a compressed exponential. Finally $\beta < 0.5$ corresponds to a stretched exponential.

In the structure factor the pair-correlation function is convoluted with the finite-size effect. The result is illustrated in Fig. 5. The correlation function dominates at small $z$ values leading to the asymptotic power-law equation (9) for the structure factor at large $q$ values. In the vicinity of a reciprocal lattice vector the finite-size contribution dominates, resulting in a Gaussian→Lorentzian line shape for a $\beta$ variation 1→0.5. If the domains are relatively large with about the same size [see Fig. 5(a)] we can expect pronounced algebraic tails in the x-ray line shape. For smaller-size domains clear deviations from the Caillé correlation will occur already at small $z$ values. This is also the case for higher harmonics and/or for large $\eta$ [compare Fig. 5(b) with Fig. 5(a)],

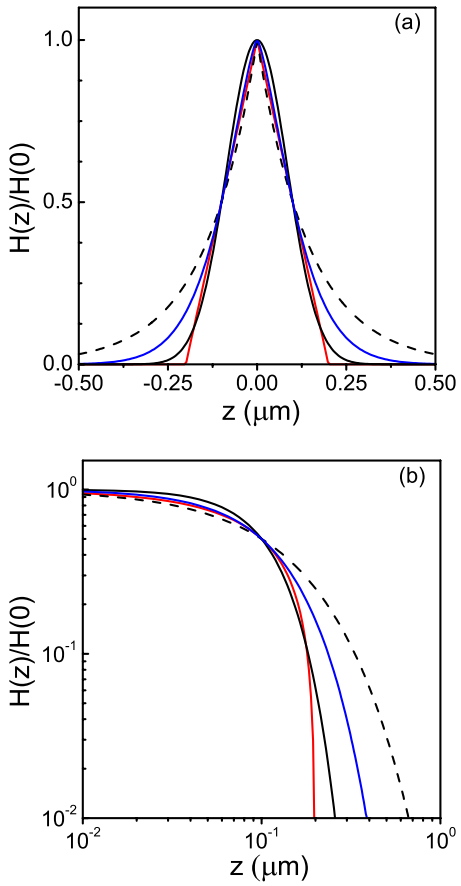


FIG. 4. (Color online) Finite-size contributions to the line shape in a linear (a) and a double logarithmic plot (b). From inside to outside: domains with sharp boundaries; Gaussian ($\beta$=1.0); stretched Gaussian ($\beta$=0.7); dashed-dotted line, exponential ($\beta$=0.5; Lorentzian in $q$ space).

especially if $\beta$ is close to 0.5 (approaching a Lorentzian). In principle such effects can obscure the asymptotic power-law behavior of the line shape. Nevertheless, even then the Caillé correlation function plays an important role in determining

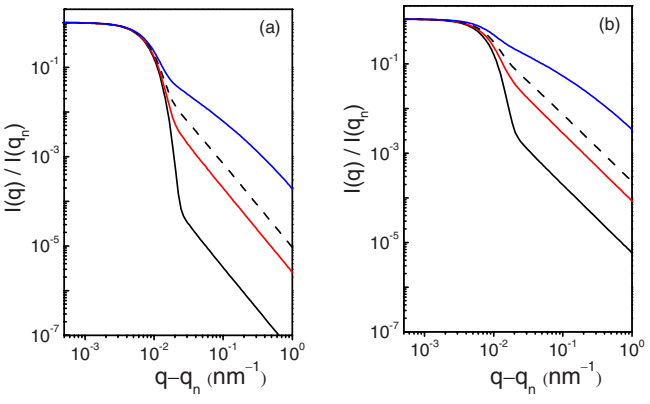


FIG. 5. (Color online) Model profiles for the first-order [(a) $\eta$=0.12] and second-order [(b) 4$\eta$=0.48] x-ray peaks for different mosaic distributions. From top to bottom: $\sigma_{\rho}$=0.5, 0.1, 0.05, 0.005. Finite-size contribution fixed to $\Delta q_z$=0.01 nm$^{-1}$ (corresponding domain size 0.6 $\mu$m).

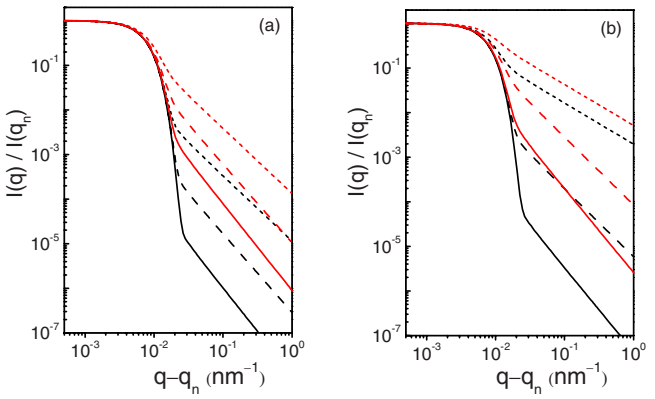


FIG. 6. (Color online) Model profiles for three harmonics for $\eta$=0.06 (a) and $\eta$=0.12 (b) and two different mosaic distributions. Solid lines, first order; dashed lines, second order; dotted lines, third order. Top lines, $\sigma_\rho$=0.005; lower lines, $\sigma_\rho$=0.05. Finite-size contribution fixed to $\Delta q_z$=0.01 nm$^{-1}$ (corresponding to 0.6 $\mu$m).

the large-$q$ tails of the line shape, especially for the higher-order peaks.

So far we considered a perfectly aligned sample, but in practice the normal's to the smectic layers are distributed around their average value. This mosaic distributions can be described by a Gaussian with a characteristic width $\phi_{\text{mos}}$ leading to the additional factor $F(\rho)$ in Eq. (12). The mosaic factor can be easily calculated for a relatively narrow distribution [33],

$$F(\rho) = \exp[-(q_n \phi_{\text{mos}} \rho/4)^2]. \tag{21}$$

Assuming the distributions of the layer normal's and of the finite domain sizes to be independent, the total in-plane effect can be combined into

$$F(\rho)H(\rho) \to \exp\left(-\frac{(\sigma_\rho \rho)^2}{2}\right). \tag{22}$$

Though the mosaic effect is dominant, when fitting the total line shape an in-plane FWHM can result that is slightly larger than the experimentally measured mosaic distribution.

The mosaic distribution sets a characteristic wave vector $q_c = \lambda q_n^2 \phi_{\text{mos}}^2/4$ [33] that determines its effect on the line shape. For a small mosaic distribution (up a few degrees) the overall effect consists of tail rising and a slight increase of the FWHM, especially for the higher harmonics (see Fig. 5). In this case the characteristic wave number $q_c$ is well inside the region limited by the finite domain sizes ($\Delta q_z$). As a consequence a clear asymptotic slope $2-n^2\eta$ can be observed. For a mosaic distribution around 10°, corresponding to the situation $q_c > \Delta q_z$, one notes a pronounced deviation from the asymptotic slope (upper lines in Fig. 5) and a less pronounced asymptotic region $1-n^2\eta$. Figure 6 indicates that typically a mosaic distribution affects all the diffraction orders mostly in the intermediate $q$ region. For a large mosaic distribution the effect will extend to large $q$ values and the Gaussian approximation used so far should be extended with next antisymmetric terms and further.

Finally there are still limitations due to measuring apparatus, which means that the intensity should be convoluted with the resolution function $R(x,y,z)$. Because of the experimental choices made so far, in most cases this point can be disregarded. Otherwise, the resolution function in the $x$ and the $y$ direction can be well approximated by Gaussians. Along the layer normal ($z$ direction) a fit can be made to the direct beam profile as measured in $q$ space, usually by the sum of Gaussian and Lorentzian functions, which is subsequently Fourier transformed to $R(z)$. Hence, we can write

$$R(x,y,z) = \exp\left(-\frac{(\sigma_x x)^2}{2} - \frac{(\sigma_y y)^2}{2}\right) R(z), \tag{23}$$

which reads in cylindrical coordinates as

$$R(x,y,z) = \exp\left(-\frac{(\sigma_x \rho)^2}{2} - \frac{(\sigma_y^2 - \sigma_x^2)\rho^2 \sin^2 \varphi}{2}\right) R(z).$$

As the resolution along the $x$ axis is negligible small (see Sec. II), $\sigma_x \ll \sigma_\rho$ and denoting $\sigma_\varphi^2 \equiv \sigma_y^2 - \sigma_x^2$ we arrive at

$$R(x,y,z) = \exp\left(-\frac{(\sigma_\varphi \rho \sin \varphi)^2}{2}\right) R(z). \tag{24}$$

Up to now the discussion has been perfectly general. The specific element to describe the cross linking in smectic elastomers relates to effects induced by the internal strain. Around the cross links, layer displacements can occur or other types of defects may be generated that are not small anymore in comparison with the layer spacing. Strain-induced broadening of x-ray peaks is well known in various fields [36–38]. Generally two effects contribute to x-ray peak broadening: the finite size of the crystalline or smectic domains and nonuniform strain within the domains induced by lattice defects. The strain broadening of a diffraction peak leads approximately to a linear increase of $\Delta q_z$ with harmonic number $n$, while the size effect does not depend on it. Hence, the measured FWHM can be written in the following way (dropping for convenience the index $z$):

$$\Delta q_{\text{expt}}^2 = \Delta q_{\text{size}}^2 + n^2 \Delta q_\epsilon^2 + \Delta q_{\text{res}}^2. \tag{25}$$

The experimentally measured FWHM is larger than the real $\Delta q_{\text{size}}$ because of a strain-induced contribution $\Delta q_\epsilon$. The resolution is added to Eq. (25) for completeness but can usually be disregarded. A critical discussion of these effects has been given in Ref. [39]. The strain-induced contribution to the line shape $I(\mathbf{q})$ can be written as

$$H_n^\epsilon(z) = \exp\left(-\frac{(n\sigma_\epsilon z)^2}{2}\right). \tag{26}$$

Now we are in a position to evaluate the intensity equation (12) for the most relevant case—scattering normal to the layers. This leads to the expression

$$I(q) \propto \int d^3\mathbf{r} G_n(\rho,z) H(\rho,z) H_n^\epsilon(z) F(\rho) R(x,y,z) \exp[i(q-q_n)z]. \tag{27}$$

Substituting all contributions, the intensity $I(q)$ can be written in cylindrical coordinates $(\rho,\varphi,z)$ as

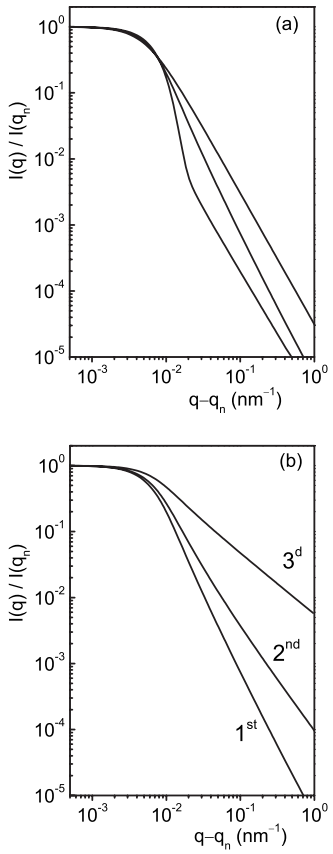


FIG. 7. Model profiles for $\eta=0.12$ and $\Delta q_z=0.01$ nm$^{-1}$ ($L=0.6$ $\mu$m). (a) First order for different values of $\beta$. From top to bottom: $\beta=0.5$; $\beta=0.7$; $\beta=1.0$. (b) Various orders for $\beta=0.7$.

$$I(q) \propto \int_{-\infty}^{\infty} dz \int_0^{\infty} d\rho\rho \int_0^{2\pi} d\varphi G_n(\rho,z) \exp\left(-\frac{(\sigma_\beta z)^{2\beta}}{2\beta} - \frac{(n\sigma_\epsilon z)^2}{2}\right) \exp\left(-\frac{(\sigma_\rho \rho)^2}{2}\right) \exp\left(-\frac{(\sigma_\varphi \rho \sin\varphi)^2}{2}\right) \times R(z) \exp[i(q-q_n)z]. \quad (28)$$

After some algebraic operations we finally arrive at

$$I(q) \propto \int_0^{\infty} dz \cos[(q-q_n)z] \exp\left(-\frac{(\sigma_\beta z)^{2\beta}}{2\beta} - \frac{(n\sigma_\epsilon z)^2}{2}\right) R(z) \int_0^{\infty} d\rho\rho G_n(\rho,z) \exp\left(-\frac{(\sigma_\rho \rho)^2}{2} - \frac{(\sigma_\varphi \rho)^2}{2}\right) I_0\left(\frac{(\sigma_\varphi \rho)^2}{2}\right), \quad (29)$$

in which $I_0$ is the modified Bessel function of zero order. We used the final expression (29) for fitting the data. Over the whole range of $q$ values the line shape is strongly affected by the contribution of the stretched Gaussian. The effect of the degree of stretching (decreasing value of $\beta$) is obvious in the tails of the peaks [Fig. 7(a)] but is diminished by the presence of a Gaussian term in the resolution function. From Fig. 7(b) we note that the stretching suppresses for all harmonic orders a clear transition from finite-size effects (central part) to Caillé tails. When for large values of $\Delta q_z$ the stretched Gaussian dominates over the other factors, the difference between first and second harmonic is small, especially for the initial decades of intensity.

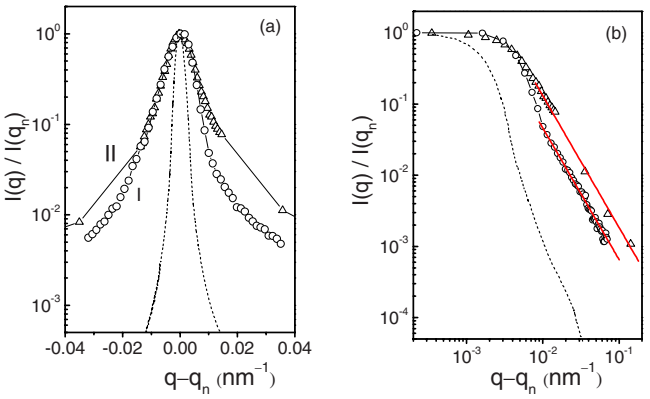


FIG. 8. (Color online) X-ray line shapes of the homopolymers I and II; the dotted line indicates the direct-beam profile. (a) Normalized intensity. (b) Double logarithmic plot of the right-hand side; the full lines correspond to $2-\eta$ with $\eta=0.15\pm0.02$.

## IV. RESULTS

In the following series of figures the x-ray line shapes of the various harmonics of the different samples will be presented in some detail. We shall systematically give combinations of two figures: first a conventional x-ray peak (intensity $I$ vs $q_z$) is shown with usually three decades of intensity displayed logarithmically. In addition a double logarithmic figure is given in which $|q-q_n|$ is displayed horizontally, thus emphasizing the behavior of the tails.

We studied homopolymer I and elastomer I for a volume fraction $x=0.05$ of cross-link V1, and homopolymer II and elastomer II for $x=0.1$, 0.15, and 0.20. In addition elastomer II has been investigated with the flexible cross-link unit V1 replaced by the stiffer cross-link V8. The x-ray scattering from homopolymer I shows one and from homopolymer II shows two harmonics originating from the smectic layering. The first-order intensity profiles are displayed in Fig. 8. The characteristic features are a central plateaulike region at small deviations from $q_n$ due to the finite size of the smectic domains, and a power-law behavior $(q_z-q_n)^{-2+\eta_n}$ at larger distances. The FWHM of the quasi-Bragg peaks is not resolution limited and the central part can be well described by a Gaussian. For the first-order peaks this indicates smectic domains along the layer normal with a finite size $L\simeq0.7$ $\mu$m for homopolymer I and 0.6 $\mu$m for homopolymer II. Away from the center of the peaks, algebraic decay is observed with an exponent $\eta_n/n^2=\eta=0.15\pm0.02$, similar as reported for other smectic polymers [17]. Intensity profiles for two harmonics of elastomer I for $x=0.05$ are shown in Fig. 9. The increase of the exponent $\eta_n$ with $n$ is well described by the scaling law $\eta_n/n^2=\eta=0.17\pm0.01$. The FWHM now leads to a finite size $L\simeq3.4$ $\mu$m, appreciably larger than for the homopolymer. The results for system I are summarized in Table

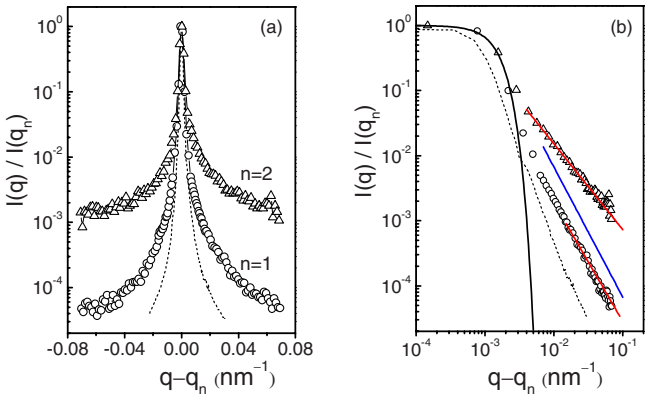


FIG. 9. (Color online) X-ray line shapes of elastomer I in a linear (a) and a double logarithmic plot (b) for a cross-link density $x=0.05$. The lines in the wings correspond to a slope $2-n^2\eta$ with $\eta=0.17\pm0.01$ and the central line to the Gaussian region. Separately a full line with a slope −2 is given; the dotted line indicates the direct beam.

I. Results for higher cross-link densities have been obtained for elastomer II; they are displayed in Figs. 10–13 and summarized in Table II. The latter results have been fully fitted using Eq. (29). To illustrate the transition we also made simple fits to the central part with all contributions set to 1 except the finite size. The latter was represented by the stretched Gaussian of Eq. (20) constrained to give the correct experimental FWHM. These results are displayed in Figs. 14 and 15 for cross-links V1 and V8, respectively.

Figure 10 shows the general features for $x=0.1$ and $x=0.15$. For $x=0.15$ the tails of the first-order and second-order peak do somewhat overlap, which complicates the analysis. Figure 11 shows three orders of diffraction for $x=0.1$. Interestingly the peak width $\Delta q_z$ increases about linearly with the harmonic number $n$ (see Table II). The experimental FWHM of the first-order peak indicates a domain size $L\simeq1.3$ $\mu$m, still somewhat larger than for the homopolymer, but clearly smaller than for $x=0.05$. In the tails of the peak, algebraic decay is nicely preserved with $\eta_n/n^2=\eta=0.16\pm0.01$, essentially the same scaling as for $x=0.05$. With increasing cross-link concentration the transparency of the samples decreases, which is also expressed by a larger mosaic distribution and fewer higher harmonics. For $x=0.15$ two orders of diffraction are observed as displayed in Fig. 12. The algebraic decay of the positional correlations is still preserved with $\eta\simeq0.15\pm0.01$, but it is partly masked by a substantial broadening of the peak along $q_z$ and by the increased mosaic spread. The FWHM of the central Gaussian of the first harmonic indicates smectic domains as small as

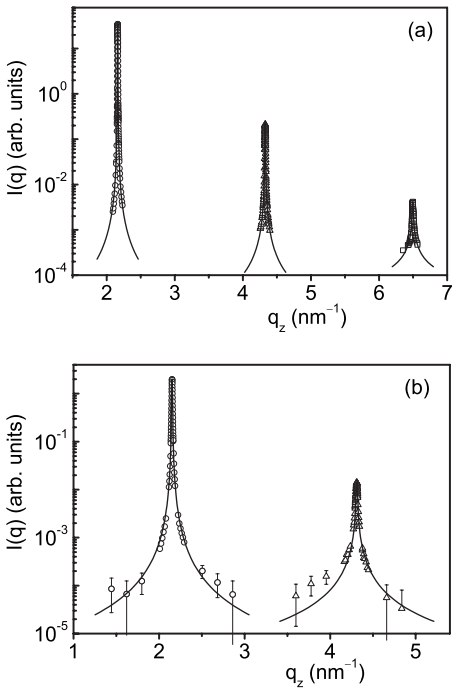


FIG. 10. Overview of x-ray line shapes of elastomer II for $x=0.1$ (a) and $x=0.15$ (b).

$L\simeq0.6$ $\mu$m. In Fig. 13 the remaining first harmonic for $x=0.2$ is compared with the ones for the other cross-link densities. It is strongly broadened both along $q_z$ (domain size about 100 nm) and along $q_x$ (mosaic distribution). From Table II we note a systematic increase of the peak width along $q_z$ both with increasing cross-link density and with the harmonic order. In Fig. 13 an additional result is included for 15% of the stiff cross-link V8, which behaves as anticipated for a concentration of the flexible cross-link V1 larger than 20%. Finally in Table III full data are given for 10%, 12.5%, and 15% of cross-link V8, which thus provides a continuation of the results observed for cross-link V1.

## V. DISCUSSION

Let us first consider Table II in some detail. At small cross-link concentration $x\leq0.05$, the finite size of the smectic domains is from 4 to 5 times larger than in the corresponding homopolymer. Evidently the elastomer network enhances the stability of the layered structure in agreement with the predictions of layer pinning theory, Eq. (10). However, within the domains the system still shows slow (algebraic) decay of the positional correlations. With increasing

TABLE I. Summary of smectic layer peak results for elastomer I and the flexible cross-link V1.

| Cross-link concentration $x$ | Harmonic order $n$ | $d\pm0.02$ (nm) | $\Delta q_z$ ($10^{-3}$ nm$^{-1}$) | Domain size $L$ ($\mu$m) | Mosaic spread (deg) |
|---|---|---|---|---|---|
| 0 | 1 | 2.78 | 8.8 | 0.71 | 1.7 |
| 0.05 | 1 | 2.88 | 2.4 | 3.4 | 0.9 |
| 0.05 | 2 | | 2.6 | | 1.3 |

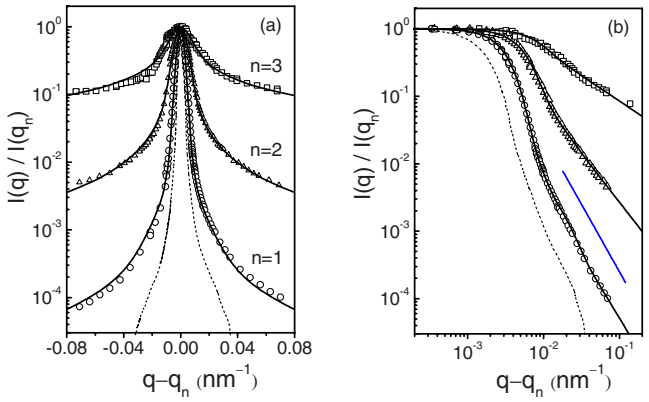


FIG. 11. (Color online) X-ray line shapes of elastomer II in a linear (a) and a double logarithmic plot (b) for a cross-link density $x=0.1$. Scaling is satisfied with $\eta=0.16\pm0.01$. Separately a full line with a slope −2 is given; the dotted line indicates the direct beam.

concentration of cross links, above $x\simeq0.1$ the disorder gradually takes over as indicated by broadening of the x-ray peak along the layer normal (Fig. 13). However, in addition the line shape also varies as illustrated in Figs. 14(a)–14(c). Going from 10% via 15% to 20% of cross-link V1 the central line shape changes from approximately Gaussian to close to Lorentzian. This is nicely expressed by the value of the exponent of the fitted stretched Gaussian correlation function, Eq. (20), that varies from $\beta=0.96\simeq1$ (pure Gaussian) for $x=0.1$ via $\beta=0.66$ for $x=0.15$ to $\beta=0.59$ (already close to 0.5) for $x=0.20$. Most importantly this trend is continued by the results for the stiff cross-link V8 (Fig. 15). The result for 10% of the stiff cross-link V8 is close to the situation for 20% of the flexible cross-link V1. As for 10% V8 we find $\beta=0.51$, in fact a fit with variable $\beta$ cannot be distinguished anymore from a pure Lorentzian ($\beta=0.5$). Upon increasing the concentration of V8 the exponent $\beta$ decreases further. For 12.5% we find $\beta=0.47$ and for 15% we arrive at $\beta=0.44$ corresponding to stretched exponential correlation functions. At this stage we cannot give a precise interpretation, but we note that a stretched exponential can be related to an average over dimensions varying over a broad range. A compressed exponential (or equivalently a stretched Gaussian) is often in a loose way associated with cooperative behavior (see, for example, [40,41]). Summarizing we encounter a gradual transition from well-distinguishable finite-size domains (flexible cross links; Gaussian) to an average over a broad range of sizes that leads first to a Lorentzian (large density of flexible cross links; medium density of rigid cross links) and subsequently to a stretched Lorentzian (large density of rigid cross links) This behavior constitutes a major theoretical challenge we cannot solve at this stage.

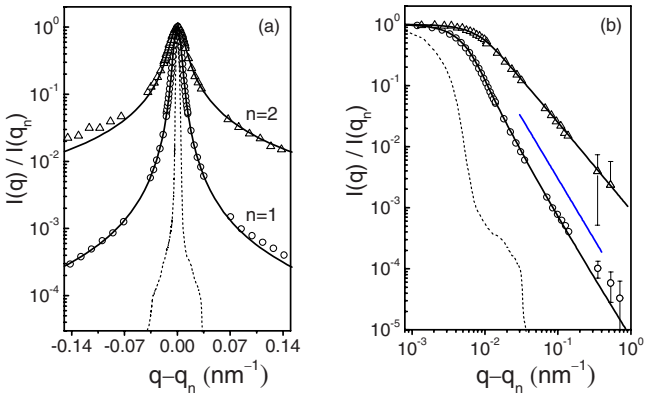


FIG. 12. (Color online) X-ray line shape of elastomer II in a linear (a) and a double logarithmic plot (b) for $x=0.15$. Scaling is satisfied with $\eta=0.16\pm0.01$. Separately a full line with a slope −2 is given; the dotted line indicates the direct beam.

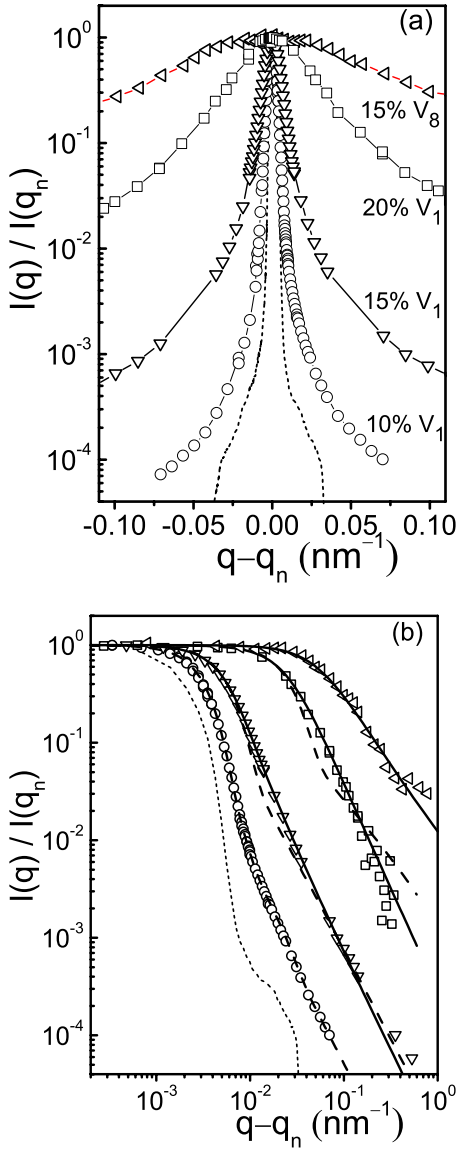


FIG. 13. (Color online) First-order diffraction of elastomer II in a linear (a) and a double logarithmic plot (b) with flexible cross-linker V1 for $x=0.1$, 0.15, and 0.2, respectively, and for $x=0.15$ with rigid cross-linker V8. The dotted line corresponds to the direct beam. In (b) the dashed lines show the best fit to the data for fixed $\beta=1.0$ (Gaussian finite size); full lines correspond to the best fit to Eq. (29).

TABLE II. Summary of smectic layer peak results for elastomer II with the flexible cross-link V1.

| Cross-link concentration $x$ | Harmonic order $n$ | $d \pm 0.02$ (nm) | $\Delta q_z$ ($10^{-3}$ nm$^{-1}$) | Domain size $L$ ($\mu$m) | Mosaic spread (deg) |
|---|---|---|---|---|---|
| 0 | 1 | 2.87 | 10.1 | 0.62 | 1.5 |
| 0 | 2 | | 12 | | 3.3 |
| 0.1 | 1 | 2.90 | 5.5 | 1.3 | 2.7 |
| 0.1 | 2 | | 10.7 | | 2.8 |
| 0.1 | 3 | | 25.5 | | 3.5 |
| 0.15 | 1 | 2.92 | 10.5 | 0.6 | 6.3 |
| 0.15 | 2 | | 25.5 | | 6.9 |
| 0.2 | 1 | 2.92 | 49 | 0.12 | 20 |

Next we come to the full fit to Eq. (29) of the experimental line shapes as given in Figs. 11–13. In Figs. 11 and 12 the asymptotic behavior away from the center of the peak can still be described by the Caillé limit, Eq. (9). The theoretically predicted scaling is well observed with a constant value $\eta=0.16\pm0.02$ for all V1 cross-link concentrations. Upon further broadening of the peaks this limit become less clear. Nevertheless the full fits indicate still an appreciable contribution of the Caillé correlation function. In Fig. 11 for $x=0.1$ the first and second order were fitted simultaneously with $\beta=1.0$ and only four additional parameters, $\eta$, $\lambda$, $\sigma_\beta$, and $\sigma_\epsilon$. The resulting values were used to calculate the third-order peak, giving an excellent fit (see Fig. 11). Additionally we made the best fit to the three first-order diffraction peaks of the elastomer II and cross-link V1 [red lines in Fig. 13(b)] with $\beta=1.0$. For the first order of diffraction we can disregard strain-induced broadening; hence only three adjustable parameters are left. Increasing the cross-link concentration tends to change the shape of the central part, although Caillé tails remain. Apparently for $x=0.15$ one should not fix $\beta$ anymore. In Fig. 12 we present results for this elastomer. Only two orders of diffraction are observed, but we could use the results for $x=0.1$ for $\lambda$ thus reducing the number of the variables. Finally we fitted the data for high cross-link densities (results in Table IV). Although the $\beta$ values from full fits deviate slightly from those obtained by a finite-size fit of the central part only, the gradual transition from $\beta=1.0\rightarrow0.5\rightarrow<0.5$ is essentially the same.

For the higher orders $n$ of the quasi-Bragg peak the width along $q_z$ increases about linearly with $n$ (compare Table II for 10% and 15% cross links), in agreement with Eq. (25). In a simple harmonic description the width of the smectic peaks would be the same for all different orders of diffraction. As mentioned in the final part of Sec. III B finite-size broadening of the x-ray peak does not depend on the order of the reflection, while the strain effect is proportional to the length of the scattering vector. Using Eq. (25) we can separate the two contributions and obtain an average domain size. The observed strain effect on the width of the quasi-Bragg peaks in smectic elastomers can be attributed to layer displacements around the cross links (or other types of topological defects generated in the presence of cross links) that are not small anymore in comparison with the layer spacing. The behavior resembles the predictions for an elastic field of distant dislocations or other topological defects [33]. Similar possibilities have been discussed for various defect situations by Krivoglaz [38].

An important source of nonuniform strain in smectic domains is due to edge dislocations that have been observed in smectic side-chain polymers by high-resolution electron microscopy [42]. We expect such dislocations to be generated in large amounts in smectic elastomers starting from a certain density of randomly distributed cross links. Such dislocations destroy the algebraic decay of the smectic layer correlations at large distances and lead to a broadening of the Gaussian-type Bragg peak [33] in dependence of the density

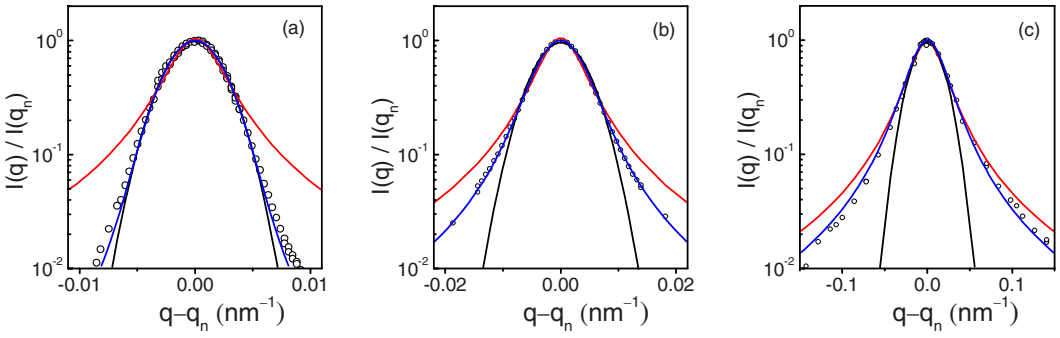


FIG. 14. (Color online) Central part only of the first-order diffraction of elastomer II with flexible cross-linker V1 for (a)–(c) $x=0.1$, 0.15, and 0.2, respectively. From outside to inside: Lorentzian fit; Gaussian; stretched Gaussian with (a)–(c) $\beta=0.96$, 0.66, and 0.59, respectively. The Lorentzian in (c) corresponds to a correlation length of $\xi\approx45$ nm.

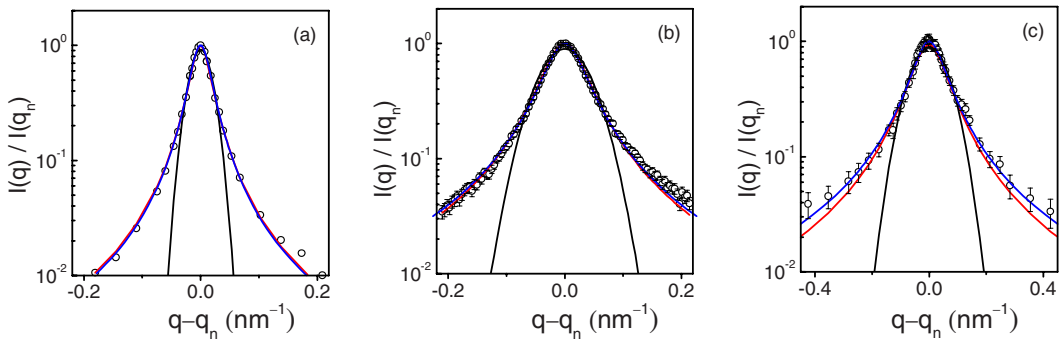


FIG. 15. (Color online) Central part only of the first-order diffraction of elastomer II with the stiff cross-linker V8 for (a)–(c) $x=0.1$, 0.125, and 0.15, respectively. From outside to inside: stretched Gaussian with (a)–(c) $\beta=0.51$, 0.47, and 0.44, respectively; Lorentzian fit; Gaussian. In (a) the Lorentzian and the stretched Gaussian coincide; in (b) the Lorentzian is just slightly lower. The Lorentzian in (a)–(c) corresponds to correlation length of $\xi \approx 53$, 26, and 15 nm, respectively.

of dislocations $N_d$. The width of the peak along $q_z$ is independent of the domain size and scales as $\Delta q_z \sim n^{4/3}$. The broadening in the transverse direction $\Delta q_x \sim q_n N_d^{1/2} L^{1/4}$ corresponds to an apparent mosaic distribution $\phi=\Delta q_x/q_n$. The broadening of the mosaic spread with increasing cross-link density from Table II allows to estimate the relative increase of the dislocation density $N_d \sim \phi^2/L^{1/2}$. Taking $L$ values from Table II we find that the dislocation density increases by a factor of about 100 when the cross-link concentration changes from zero to 20%. Even though these estimates are very approximate, they do give the right order of magnitude of multiplication of dislocations. Another obvious reason for peak broadening along $q_x$ is the diminishing finite size with increasing cross-link density of the domains in the smectic layer planes. The above factors contribute to the total width of the smectic peak in the transverse direction.

Though the observed behavior is consistent with the general predictions for random quenched disorder, it is remarkable that the algebraic decay survives up to large cross-link densities. The analogy might fail because in smectic elastomers the cross links are not fully frozen defects, but consist of flexible chains embedded in the slowly fluctuating elastomer network. Clearly this makes the situation different from the type of quenched disorder introduced in aerogel or aerosil networks. We speculate that starting from a certain concentration of cross links, defects of higher strength are generated in a large amount, which causes large displacements of the layers, $qu \gg 1$. The elastic field of such defects, for example, dislocation loops, could suppress the Bragg peaks and lead increasingly to diffuse scattering with a Lorentzian-type shape.

In conclusion we have used high-resolution x-ray scattering to determine the positional correlations in smectic elastomers with increasing number of cross links. The smectic line shapes are described by the Caillé correlation function convoluted with a finite-size factor represented by a stretched Gaussian. At small cross-link concentration the elastomer network enhances the stability of the smectic structure against layer displacement fluctuations. At higher concentrations a transition to disorder is reflected in the x-ray line shape by a change in the exponent of a stretched Gaussian from 1 (simple Gaussian describing finite-size domains) to 0.5 (Lorentzian describing extended short-range correlations). For a flexible cross link the algebraic decay of positional correlations survives in domains of decreasing size up to relatively large concentrations exceeding 15%. The observed broadening of the higher harmonics of the x-ray peak indicates nonuniform strain within finite-size smectic domains. For a concentration of about 20% the smectic ordering is destroyed by the random field of cross links and replaced by extended short-range correlations. For a stiff cross link the smectic layering is lost already at $<10\%$ and for increasing concentration the remaining correlations can be described by a stretched exponential. A new theoretical concept regarding disordering by a random internal field is needed which incorporates that in smectic elastomers the defects are cross links consisting of flexible chains embedded in a fluctuating layered system.

## ACKNOWLEDGMENTS

The authors thank Heino Finkelmann (Freiburg) for continuous stimulating interactions, Elke Stibal-Fischer

TABLE III. Summary of smectic layer peak results for elastomer II with the rigid cross-link V8.

| Cross-link concentration $x$ | Harmonic order $n$ | $d \pm 0.02$ (nm) | $\Delta q_z$ ($10^{-3}$ nm$^{-1}$) | Domain size $L$ ($\mu$m) | Mosaic spread (deg) |
|---|---|---|---|---|---|
| 0.10 | 1 | 2.81 | 44 | 0.14 | 17 |
| 0.125 | 1 | 2.82 | 99 | 0.06 | 29 |
| 0.15 | 1 | 2.77 | 152 | 0.04 | 50 |

TABLE IV. Fitting results for the smectic layer peak of elastomer II with the flexible cross-link V1.

| Cross-link concentration $x$ | $\beta$ | $\sigma_\beta$ ($10^{-3}$ nm$^{-1}$) | $\sigma_\epsilon$ ($10^{-3}$ nm$^{-1}$) | $\eta$ | $\lambda$ (nm) |
|---|---|---|---|---|---|
| 0.10 | 1.00 | $1.70 \pm 0.05$ | $0.73 \pm 0.04$ | $0.15 \pm 0.01$ | $0.50 \pm 0.05$ |
| 0.15 | $0.68 \pm 0.03$ | $2.6 \pm 0.4$ | $2.7 \pm 0.3$ | $0.16 \pm 0.02$ | 0.5 |
| 0.20 | $0.62 \pm 0.03$ | $20 \pm 1$ | | $0.16 \pm 0.06$ | 0.5 |

(Freiburg) for preparation of the elastomers, Vladimir Kaganer (Berlin) for valuable discussions, Dinitza Lambreva (Amsterdam) for taking part in the early measurements, and Steve Bennett (NSLS, Brookhaven) for local support at beamline X10A. This work is part of the research program of the Stichting voor Fundamenteel Onderzoek der Materie (FOM), which is financially supported by the Nederlandse Organisatie voor Wetenschappelijk Onderzoek (NWO).

[1] G. Blatter, M. V. Feigel'man, V. B. Geshkenbein, A. I. Larkin, and V. M. Vinokur, Rev. Mod. Phys. **66**, 1125 (1994).
[2] D. S. Fisher, M. P. A. Fisher, and D. A. Huse, Phys. Rev. B **43**, 130 (1991).
[3] R. J. Birgeneau, J. Magn. Magn. Mater. **177-181**, 1 (1998).
[4] M. Chan, N. Mulders, and J. Reppy, Phys. Today **49**(8), 30 (1996).
[5] T. Bellini, L. Radzihovsky, J. Toner, and N. Clark, Science **294**, 1074 (2001).
[6] A. I. Larkin, Sov. Phys. JETP **31**, 784 (1970).
[7] A. I. Larkin and Y. N. Ovchinikov, J. Low Temp. Phys. **34**, 409 (1979).
[8] T. Giamarchi and P. Le Doussal, Phys. Rev. B **52**, 1242 (1995).
[9] P. M. Chaikin and T. C. Lubensky, *Principles of Condensed Matter Physics* (Cambridge University Press, Cambridge, 1995).
[10] L. D. Landau, Phys. Z. Sowjetunion **11**, 545 (1937).
[11] R. E. Peierls, Helv. Phys. Acta **7**, 81 (1934).
[12] A. Caillé, C. R. Seances Acad. Sci., Ser. B **274**, 891 (1972).
[13] J. Als-Nielsen, J. D. Litster, R. J. Birgeneau, M. Kaplan, C. R. Safinya, A. Lindegaard-Andersen, and S. Mathiesen, Phys. Rev. B **22**, 312 (1980).
[14] C. R. Safinya, D. Roux, G. S. Smith, S. K. Sinha, P. Dimon, N. A. Clark, and A. M. Bellocq, Phys. Rev. Lett. **57**, 2718 (1986).
[15] D. Roux and C. R. Safinya, J. Phys. (France) **49**, 307 (1988).
[16] D. C. Wack and W. W. Webb, Phys. Rev. A **40**, 1627 (1989).
[17] E. Nachaliel, E. N. Keller, D. Davidov, and C. Boeffel, Phys. Rev. A **43**, 2897 (1991).
[18] P. Štěpánek, F. Nallet, O. Diat, K. Almdal, and P. Panine, Macromolecules **35**, 7287 (2002).
[19] R. L. Leheny, S. Park, R. J. Birgeneau, J. L. Gallani, C. W. Garland, and G. S. Iannacchione, Phys. Rev. E **67**, 011708 (2003).
[20] Z. Kutnjak, S. Kralj, G. Lahajnar, and S. Zumer, Phys. Rev. E **68**, 021705 (2003);
[21] D. Liang and R. L. Leheny, Phys. Rev. E **75**, 031705 (2007).
[22] L. Radzihovsky and J. Toner, Phys. Rev. Lett. **79**, 4214 (1997).
[23] L. Radzihovsky and J. Toner, Phys. Rev. B **60**, 206 (1999).
[24] M. Warner and E. M. Terentjev, *Liquid Crystal Elastomers* (Clarendon, Oxford, 2003).
[25] H. Finkelmann, E. Nishikawa, G. G. Pereira, and M. Warner, Phys. Rev. Lett. **87**, 015501 (2001).
[26] E. M. Terentjev, M. Warner, and T. C. Lubensky, Europhys. Lett. **30**, 343 (1995).
[27] M. J. Osborne and E. M. Terentjev, Phys. Rev. E **62**, 5101 (2000).
[28] G. C. L. Wong, W. H. de Jeu, H. Shao, K. S. Liang, and R. Zentel, Nature (London) **389**, 576 (1997).
[29] P. D. Olmsted and E. M. Terentjev, Phys. Rev. E **53**, 2444 (1996).
[30] E. M. Terentjev, Macromol. Symp. **117**, 79 (1997).
[31] D. M. Lambreva, B. I. Ostrovskii, H. Finkelmann, and W. H. de Jeu, Phys. Rev. Lett. **93**, 185702 (2004).
[32] E. Nishikawa and H. Finkelmann, Macromol. Rapid Commun. **18**, 65 (1997).
[33] V. M. Kaganer, B. I. Ostrovskii, and W. H. de Jeu, Phys. Rev. A **44**, 8158 (1991).
[34] B. E. Warren, Phys. Rev. **59**, 693 (1941).
[35] J. I. Langford, D. Louër, and P. Scardi, J. Appl. Crystallogr. **33**, 964 (2000).
[36] B. E. Warren and B. L. Averbach, J. Appl. Phys. **21**, 595 (1950).
[37] G. K. Williamson and W. H. Hall, Acta Metall. **1**, 22 (1953).
[38] M. Krivoglaz, *X-ray and Neutron Diffraction in Non-Ideal Crystals* (Springer, Berlin, 1996).
[39] V. M. Kaganer, O. Brandt, A. Trampert, and K. H. Ploog, Phys. Rev. B **72**, 045423 (2005).
[40] J.-P. Bouchaud, in *Anomalous Transport: Foundations and Applications*, edited by G. Radons, I. M. Sokolov, and R. Klages (Wiley, 2008).
[41] P. Falus, M. A. Borthwick, S. Narayanan, A. R. Sandy, and S. G. J. Mochrie, Phys. Rev. Lett. **97**, 066102 (2006).
[42] I. G. Voigt-Martin, H. Krug, and D. van Dyck, J. Phys. (France) **51**, 2347 (1990).